*mathematics*

MDPI

*Article*

# Modeling Demographic Noise in Discrete and Continuous Settings

**Roberto Macrelli [1,*] and Margherita Carletti [2]**

[1] DISB Department, University of Urbino C. Bo, Via Sant'Andrea 34, 61029 Urbino, Italy
[2] DISPeA Department, University of Urbino C. Bo, Piazza Della Repubblica 13, 61029 Urbino, Italy
* Correspondence: roberto.macrelli@uniurb.it

**Abstract**

In this paper, we numerically compare two distinct techniques for modeling demographic noise in biomathematical systems: the *forward* method introduced by Allen, which starts from discrete stochastic processes and moves forward to their continuous counterparts, and the *backward* technique introduced by Carletti and Banerjee, which models discrete stochastic processes incorporating intrinsic noise by moving backward from ordinary differential equation (ODE) systems. Our work highlights that the two methods show consistent dynamical trends. Nevertheless, the backward technique offers greater ease of use and provides a wider range of applications, as it allows researchers to infer demographic stochasticity directly from systems previously modeled by standard ODEs.

**Keywords:** biomathematical modelling; demographic noise; chemical kinetics; numerical simulations

**MSC:** 60H35; 92-10; 92-08

## 1. Introduction

Dynamical systems formulated through deterministic differential equations constitute idealized frameworks that neglect stochastic influences. In biomathematical modeling, a fundamental distinction is made between environmental (extrinsic) noise and demographic (intrinsic) noise. The latter accounts for vital events such as births, deaths, immigration, and emigration, attributing temporal fluctuations to the intrinsic demographic variations within interacting populations. The literature thoroughly documents the modeling and simulation of demographic noise as stochastic processes operating at the individual level, typically formulated as discrete stochastic systems [1]. For large population sizes, these discrete stochastic processes converge to continuous stochastic ordinary differential equations (SODEs); if noise is negligible, they reduce to standard ordinary differential equation (ODE) models. This approach has been extensively addressed in the monograph by Allen [2].

Conversely, a major challenge lies in the inverse process: deducing the impact of demographic noise on a natural system originally described by a set of ODEs. This backward framework was introduced more recently by Carletti and Banerjee [3].

Traditionally, the incorporation of intrinsic noise requires knowledge of discrete individual counts. A prominent framework for this purpose is the forward approach developed by Allen [2], which treats populations as discrete integer entities rather than continuous densities. Species interactions are modeled by taking the limit as the time step $\Delta t \to 0$, transitioning from discrete-time Markov chains to continuous-time Markov chain (CTMC) processes. This formulation ultimately leads to a system of SODEs, which are subsequently simulated using standard numerical methods.

Check for updates

Academic Editors: Cristina Januário and Jorge Duarte

Received: 10 August 2026
Revised: 7 October 2026
Accepted: 9 October 2026
Published: 11 October 2026

**Copyright:** © 2026 by the authors. Licensee MDPI, Basel, Switzerland. This article is an open access article distributed under the terms and conditions of the Creative Commons Attribution (CC BY) license.

However, significant limitations arise in practical applications: the scientific literature and empirical data are overwhelmingly dominated by continuous deterministic frameworks, such as ODEs expressed in terms of continuous densities, rather than discrete units. For example, in fields ranging from bacteriophage–host interactions to epidemic spread, well-established ODE models already exist, whereas discrete empirical data are often unavailable.

To address this gap, the alternative "backward" approach [3] can be implemented. Instead of deriving continuous stochasticity from a discrete baseline, the backward method initiates from a well-defined deterministic ODE. It reconstructs the discrete stochastic process underlying the given ODE by using the same framework as in chemical kinetic models. This approach treats demographic noise as the ecological equivalent of the stochastic modeling used in Gene Regulatory Networks (GRNs) [4]. Usually, simulations of such discrete chemical reaction networks are performed via Stochastic Simulation Algorithms (SSAs), assuming small, integer molecular counts. The pioneering probabilistic simulation algorithm developed by Gillespie [5] provides a rigorous numerical procedure for simulating the time evolution of a well-mixed, homogeneous reacting system while accounting for its inherent randomness.

This paper aims to compare the forward and backward approaches. Specifically, we examine whether the backward reconstruction yields statistically consistent results compared to Allen's established method when applied to identical biological phenomena, namely the Susceptible–Infected–Susceptible (SIS) [2] bacterial interaction. We investigate the adaptability of both frameworks, considering that the backward approach can offer a more versatile and structurally viable alternative for the study of demographic noise, given the vast repository of existing continuous ODE literature. Crucially, while both frameworks are rooted in analytically related formulations, our comparative analysis systematically disentangles purely algorithmic numerical artifacts from the fundamental structural limitations that emerge within the continuous diffusion approximation under finite population sizes near absorbing states.

## 2. Mathematical Frameworks and Model Formulations

### *2.1. Allen's Method*

In this paper, we are interested in investigating the impact of demographic noise on the well-known Susceptible–Infected–Susceptible (SIS) epidemic model. The system describes the infection of susceptible individuals, who become infected, and their subsequent possible reinfection due to waning immunity. The deterministic model equations are given by

$$\begin{cases} \frac{dS(t)}{dt} = -\frac{\beta}{N}S(t)I(t)+\gamma I(t) \\ \frac{dI(t)}{dt} = \frac{\beta}{N}S(t)I(t)-\gamma I(t) \end{cases}. \quad (1)$$

where $S(t)$ and $I(t)$ denote the densities of the susceptible and infected populations at time $t$, respectively. The parameter $\beta > 0$ represents the contact or transmission rate, which is the average number of adequate contacts per unit time that lead to infection. The parameter $\gamma > 0$ denotes the recovery rate, i.e., the rate at which infectious individuals recover, and $N = S(t) + I(t)$ is the constant total population density. The term $\beta S(t)I(t)/N$ represents the rate at which the susceptible density becomes infected, while $\gamma I(t)$ represents the rate of density moving back to the susceptible class.

The initial condition for the system can be any positive point in $R^2$. The behavior of the solution of these ODEs depends on the values of parameters $\beta$ and $\gamma$ (see Appendix A). Let $k = \gamma/\beta$. By scaling the system variables by the total population density $N$, it is straightforward to show that the disease-free equilibrium, expressed in terms of

population fractions as $E_0 = (1,\ 0)$, always exists. Furthermore, if $k \geq 1$, the equilibrium $E_0 = (1, 0)$ is globally asymptotically stable, meaning the disease dies out. Conversely, if $0 < k < 1$, a positive endemic equilibrium $E_+ = (k, 1-k)$ emerges and is globally asymptotically stable.

In a deterministic setting, whether the disease spreads and leads to an epidemic depends on the basic reproduction number, $R_0$, defined as

$$R_0 = \frac{\beta}{\gamma} = \frac{1}{k}. \tag{2}$$

An epidemic occurs in the supercritical regime when $R_0 > 1$, leading to a unique endemic equilibrium, whereas the disease dies out in the subcritical regime when $R_0 < 1$. The critical threshold regime occurs precisely when $R_0 = 1$. To capture the underlying demographic stochasticity, we shift our focus from the continuous densities $S(t)$ and $I(t)$ to the discrete state variables that represent individual counts.

Following Allen [2], we construct a continuous-time Markov chain (CTMC) model [6,7] for the SIS system based on the ODE model (1). Let $Y_1(t)$ and $Y_2(t)$ be two discrete random variables representing the number of susceptible and infected individuals at time $t$, respectively. The random variables $Y_i(t)$ $(i = 1, 2,\ t > 0)$ take non-negative integer values. Assuming fixed initial values, $Y_1(0) = n_{10} > 0$ and $Y_2(0) = n_{20} > 0$, the joint probabilities associated with the bivariate process $\{(Y_1(t), Y_2(t))\}$ are defined as $p_{n_1,n_2}(t) = Prob\{Y_1(t) = n_1, Y_2(t) = n_2 | Y_1(0) = n_{10}, Y_2(0) = n_{20}\}$.

Let $\Delta Y_i(t) \equiv Y_i(t + \Delta t) - Y_i(t)$, where $\Delta t$ is chosen small enough such that $\Delta Y_i \in \{-1, 0, 1\}$, $i = 1, 2$. We assume that the probability of multiple transitions occurring within $\Delta t$ is negligible, and we denote it as $o(\Delta t)$. Transmission occurs via a direct transfer from the susceptible to the infected class upon infection, and individuals return to the susceptible class upon recovery. The infinitesimal transition probabilities for the continuous-time Markov chain model are given by

$$Prob\{\Delta Y_1 = i, \Delta Y_2(t) = j | Y_1 = n_1, Y_2 = n_2\} = \begin{cases} \gamma n_2 \Delta t + o(\Delta t) & (i,j) = (1,-1) \\ \frac{\beta}{N} n_1 n_2 \Delta t + o(\Delta t) & (i,j) = (-1,1) \\ 1 - \left(\gamma n_2 + \frac{\beta}{N} n_1 n_2\right)\Delta t + o(\Delta t) & (i,j) = (0,0) \\ o(\Delta t) & otherwise \end{cases} \tag{3}$$

The probabilities $p_{n_1,n_2}(t)$ satisfy the forward Kolmogorov differential equation [2]:

$$\frac{dp_{n_1,n_2}(t)}{dt} = \frac{\beta}{N}(n_1+1)(n_2-1)p_{n_1+1,n_2-1}(t) + \gamma(n_2+1)p_{n_1-1,n_2+1}(t) + -\left(\frac{\beta}{N} n_1 n_2 + \gamma n_2\right) p_{n_1,n_2}(t). \tag{4}$$

Furthermore, following Allen [2], the boundary conditions satisfy

$$\begin{array}{c} \frac{dp_{n_1,0}(t)}{dt} = \gamma p_{n_1-1,1}(t), \\ \frac{dp_{0,n_2}(t)}{dt} = \frac{\beta}{N}(n_2-1)p_{1,n_2-1} - \gamma n_2 p_{0,n_2}(t), \\ \frac{dp_{0,0}(t)}{dt} = 0. \end{array} \tag{5}$$

The moments of the bivariate process can be derived from the forward Kolmogorov equation (Equation (4)). The moment-generating function is given by [2,6,7]

$$M(z_1, z_2, t) = \sum_{n_1=0}^{\infty} \sum_{n_2=0}^{\infty} p_{n_1,n_2}(t) e^{n_1 z_1} e^{n_2 z_2} \tag{6}$$

for some $z_1, z_2 \in R$. By differentiating $M$ with respect to $t$ and applying (4), it can be shown that the moment-generating function satisfies the following partial differential equation [2]:

$$\frac{\partial M(z_1, z_2, t)}{\partial t} = \frac{\beta}{N}(e^{z_2 - z_1} - 1)\frac{\partial^2 M}{\partial z_1 \partial z_2} + \gamma(e^{z_1 - z_2} - 1)\frac{\partial M}{\partial z_2} \tag{7}$$

Differentiating both sides of (7) with respect to $z_1$ and applying the product rule, we obtain

$$\frac{\partial^2 M(z_1, z_2, t)}{\partial z_1 \partial t} = \frac{\beta}{N}\left[-e^{z_2 - z_1}\frac{\partial^2 M}{\partial z_1 \partial z_2} + (e^{z_2 - z_1} - 1)\frac{\partial^3 M}{\partial z_1^2 \partial z_2}\right] + \gamma\left[e^{z_1 - z_2}\frac{\partial M}{\partial z_2} + (e^{z_1 - z_2} + -1)\frac{\partial^2 M}{\partial z_1 \partial z_2}\right]. \tag{8}$$

Substituting $z_1 = z_2 = 0$ in (8) yields the following differential equation for the first moment (or expected value) of $Y_1$,

$$\frac{dE(Y_1(t))}{dt} = -\frac{\beta}{N}E[Y_1(t)Y_2(t)] + \gamma E[Y_2(t)], \tag{9}$$

where $E[Y_1(t)] = \sum_{n_1=0}^{\infty}\sum_{n_2=0}^{\infty} p_{n_1,n_2}(t)n_1$.

A similar expression can be derived for $E[Y_2(t)]$ and higher-order moments by differentiating $M$ and evaluating the derivatives at $z_1 = z_2 = 0$. For instance:

$$\frac{\partial^2 M(z_1, z_2, t)}{\partial z_2 \partial t} = \frac{\beta}{N}\left[e^{z_2 - z_1}\frac{\partial^2 M}{\partial z_1 \partial z_2} + (e^{z_2 - z_1} - 1)\frac{\partial^3 M}{\partial z_1 \partial z_2^2}\right] + \gamma\left[-e^{z_1 - z_2}\frac{\partial M}{\partial z_2} + (e^{z_1 - z_2} + -1)\frac{\partial^2 M}{\partial z_2^2}\right] \tag{10}$$

$$\frac{dE(Y_2(t))}{dt} = \frac{\beta}{N}E[Y_1(t)Y_2(t)] - \gamma E[Y_2(t)]. \tag{11}$$

It can be proven that these expectations are non-negative and retain the same properties as the variables in the deterministic model [2,7].

The Itô SODEs may be obtained by adopting standard methods [7–9] and constructing the probability table based on the continuous-time Markov chain framework (3) proposed by Allen [2]. Let $X_1(t)$ and $X_2(t)$ be random variables representing the population sizes of susceptible and infected individuals, respectively, $X_1(t),\ X_2(t) \in R^+$, and let $X(t) = (X_1(t), X_2(t))^T$ denote the joint random vector.

As in the continuous-time Markov chain model, we assume that the time interval $\Delta t$ is sufficiently small, so that at most one change between the susceptible and infected states occurs within this time interval. Let $\Delta X(t) = (\Delta X_1(t), \Delta X_2(t))^T$, where $\Delta X_i(t) = X_i(t + \Delta t) - X_i(t)$ $(i = 1, 2)$ represents the incremental change in the two populations during the time interval $\Delta t$.

The possible changes are summarized in Table 1, consistent with the continuous-time Markov chain model (3).

**Table 1.** Possible changes in $\Delta X$.

| $\Delta X(t)$ | Probability $P_i \Delta t$ |
|---|---|
| $(1, -1)^T$ | $p_1 = \gamma X_2 \Delta t$ |
| $(-1, 1)^T$ | $p_2 = \frac{\beta X_1 X_2}{N}\Delta t$ |
| $(0, 0)^T$ | $p_3 = 1 - (\gamma X_2 + \frac{\beta X_1 X_2}{N})\Delta t$ |

For $\Delta t$ sufficiently small, it is possible to evaluate the mean using $E(\Delta X) \approx (1, -1)^T p_1 + (-1, 1)^T p_2 + (0, 0)^T p_3 = (\mu_1, \mu_2)^T \Delta t = \mu \Delta t$, where $\mu_1 = \gamma X_2 - \beta X_1 X_2 / N$ and $\mu_2 = -\gamma X_2 + \beta X_1 X_2 / N$. Furthermore, the covariance matrix for $\Delta X$ is defined as

$V = E\left[\Delta X(\Delta X)^T\right] - E(\Delta X)[E(\Delta X)]^T \approx E\left(\Delta X \Delta X^T\right)$, neglecting terms $E(\Delta X)[E(\Delta X)]^T$ of order $(\Delta t)^2$:

$$V = E\begin{pmatrix} (\Delta X_1)^2 & \Delta X_1 \Delta X_2 \\ \Delta X_1 \Delta X_2 & (\Delta X_2)^2 \end{pmatrix} \approx \begin{pmatrix} \sigma_{11} & \sigma_{12} \\ \sigma_{21} & \sigma_{22} \end{pmatrix} \Delta t \tag{12}$$

where the entries are computed by summing the contributions of all transitions:

$$\sigma_{11} = (1)^2 \gamma X_2 + (-1)^2 \beta X_1 X_2 / N, = \gamma X_2 + \beta X_1 X_2 / N,$$

$$\sigma_{22} = (-1)^2 \gamma X_2 + (1)^2 \beta X_1 X_2 / N = \gamma X_2 + \beta X_1 X_2 / N,$$

$$\sigma_{12} = \sigma_{21} = (1)(-1)\gamma X_2 + (-1)(1)\beta X_1 X_2 / N = -(\gamma X_2 + \frac{\beta X_1 X_2}{N}).$$

We can denote $V = C\Delta t$, where matrix $C$ is positive semidefinite (and singular). Consequently, evaluating the stochastic diffusion matrix $B$, which is the square root of $C$ (i.e., $B = \sqrt{C} \approx \sqrt{V/\Delta t}$), for the resulting SODE yields [2]

$$C = \begin{pmatrix} \frac{\beta X_1 X_2}{N} + \gamma X_2 & -\frac{\beta X_1 X_2}{N} - \gamma X_2 \\ -\frac{\beta X_1 X_2}{N} - \gamma X_2 & \frac{\beta X_1 X_2}{N} + \gamma X_2 \end{pmatrix}. \tag{13}$$

Following Allen [2], a closed-form expression for the square root matrix $B$ is given by

$$B = \sqrt{\frac{\frac{\beta X_1 X_2}{N} + \gamma X_2}{2}} \begin{pmatrix} 1 & -1 \\ -1 & 1 \end{pmatrix} \tag{14}$$

It can be readily verified that $B^2 = C$.

For sufficiently large values of $X(t)$, the population increment $\Delta X(t)$ can be approximated by a normal distribution with mean $\mu\Delta t$ and covariance matrix $B^2\Delta t = C\Delta t$. Assuming a bivariate standard normal vector $\eta \sim N(0,1)$, it follows that $\mu\Delta t + B\sqrt{\Delta t}\eta \sim N(\mu\Delta t, B^2\Delta t)$ [10]. Consequently, the updating formula can be expressed as $X(t+\Delta t) = X(t) + \Delta X(t) = X(t) + \mu\Delta t + B\sqrt{\Delta t}\eta$. This setup corresponds to the Euler–Maruyama numerical scheme applied to a system of Itô SODEs. As the time step $\Delta t \to 0$, and provided that a unique stochastic integral exists, the random increment $\sqrt{\Delta t}\eta$ formally converges to the Wiener increment $dW$, where $W = (W_1, W_2)^T$ represents a vector of independent standard Wiener processes.

Consequently, the discrete system converges in the mean-square sense to the system of Itô SODEs $dX = \mu dt + BdW$ [2]. In particular, the explicit Itô SODEs for the SIS model are [2]

$$\begin{aligned} dX_1 &= \left(-\tfrac{\beta}{N} X_1 X_2 + \gamma X_2\right) dt + B_{11} dW_1 + B_{12} dW_2 \\ dX_2 &= \left(\tfrac{\beta}{N} X_1 X_2 - \gamma X_2\right) dt + B_{21} dW_1 + B_{22} dW_2, \end{aligned} \tag{15}$$

where $X_1 \in [0,\ N - X_2]$ and $X_2 \in [0,\ N - X_1]$, and the components of the diffusion matrix are obtained directly from (1) as $B_{11} = B_{22} = -B_{12} = -B_{21} = \sqrt{\frac{1}{2}\left(\frac{\beta}{N} X_1 X_2 + \gamma X_2\right)}$ [2]. The existence and uniqueness of the solution for model (15) are well-established in the literature [2].

### *2.2. The Backward Technique*

Consider a mixture of $N$ molecular species $S_1,\ S_2, \ldots,\ S_N$ interacting through $M$ reaction channels within a fixed volume $\Omega$ at a constant temperature. The time evolution of this system is characterized by a discrete nonlinear Markov process. In this framework,

the state of the system at time $t$ is represented by an $N$-dimensional vector $X(t)$, whose components denote the molecule counts of each species. Because $X(t) = x$ is a discrete jump Markov process, its probability distribution over time—conditioned on an initial state $X(t_0) = x_0$—is governed by the Chemical Master Equation (CME) [5]:

$$\frac{\partial}{\partial t}P(x, t|x_0, t_0) = \sum_{j=1}^{M} a_j(x - v_j)P(x-v_j, t|x_0, t_0) - a_j(x)P(x, t|x_0, t_0). \tag{16}$$

Although the CME can be expressed as a discrete parabolic partial differential equation, it is generally analytically intractable, and numerical simulation methods are required to approximate its solution.

Any algorithmic approach used to simulate a network of chemical reactions is uniquely defined by two sets of quantities: the stoichiometric vectors $\nu_1, \ldots, \nu_M$, which represent the net change in molecule counts across the system when the $R_j$-th reaction occurs $(j = 1, \cdots, M)$; and the propensity functions $a_1(X(t)), \ldots, a_M(X(t))$, which describe the relative probability per unit time that the $R_j$-th reaction will take place given the current state $X(t)$.

In many biochemical systems, some reactions occur much faster than others and rapidly reach a local steady state. Within the framework of the standard Stochastic Simulation Algorithm (SSA) [5], the overall dynamics of the system are predominantly driven by these slow reactions. In a deterministic context, this disparity in timescales is known as "stiffness."

Furthermore, scale differences influence the choice of the modeling tool: when certain chemical species are present in small quantities, discrete stochastic modeling is essential. Conversely, if species exist in large numbers, continuous stochastic or deterministic differential equations become more appropriate. In contrast, the exact SSA treats all species uniformly as discrete stochastic processes [11]. To address this multiscale challenge, Burrage et al. [12] classified reaction networks into slow, intermediate, and fast, simulating the resulting systems using their appropriate modeling regimes. Despite its computational demands, the SSA has been successfully applied to model a wide range of biological phenomena, including lambda phage regulation [13] and circadian rhythms [14,15].

When noise effects remain non-negligible, but the system size justifies continuity arguments, one can invoke the Central Limit Theorem. By matching the first two infinitesimal moments of the CME, we can derive an SODE system that describes the continuous-time evolution of the underlying Markov process [16]. This formulation is known as the Chemical Langevin Equation (CLE) [5]:

$$dX(t) = \sum_{j=1}^{M} v_j a_j(X(t))dt + B(X(t))dW(t) \qquad X(0) = X_0 \tag{17}$$

Here, the system is driven by an $M$-dimensional stochastic process whose components, $W_i(t)$, are independent standard Wiener processes, and $B(X(t))$ is an $N \times N$ matrix satisfying

$$B(X(t))B(X(t))^T = C(X(t)) = \nu Diag(a_1(X(t)), \ldots, a_M(X(t)))v^T, \tag{18}$$

where $\nu = [\nu_1, \ldots, \nu_M]$ is the $N \times M$ stoichiometric matrix.

Stochastic simulation algorithms are inherently variable time-stepping methods. At each iteration, two random variables are sampled from a uniform distribution $U(0, 1)$ to determine both the time increment until the next event and the specific reaction channel that fires. The species populations are then updated using the corresponding stoichiometric vectors, and the process repeats.

A crucial limitation of the exact SSA arises when molecule counts are high: the time steps become exceptionally small, forcing the simulation to advance painstak-

ingly via individual, consecutive reactions. Consequently, the SSA becomes computationally prohibitive for large-scale reaction networks representing complex, biologically realistic phenomena.

When the system contains large numbers of molecules, the dynamics can be expressed in terms of continuous concentrations, validating a deterministic framework. This macroscopic, averaged behavior is described by a system of ODEs governed by the classical Law of Mass Action:

$$X'(t) = \sum_{j=1}^{M} v_j a_j(X(t)),\ X(0) = X_0. \tag{19}$$

The forward modeling pipeline—progressing from discrete stochastic systems to continuous SODEs for large populations and finally reducing to deterministic ODEs when noise is omitted—is well-established in the literature [2,17]. Conversely, the *inverse process*—inferring the underlying discrete demographic noise from a natural system initially described by ODEs—presents an intriguing challenge. Since demographic noise is the ecological counterpart of intrinsic noise in genetic regulation, we can reconstruct these underlying discrete stochastic processes by mapping the deterministic differential system back into a chemical kinetics framework.

Carletti and Banerjee [3] developed a method to systematically incorporate intrinsic noise into existing ordinary differential systems. Thus, we view our baseline ODE model as the deterministic limit of a Chemical Langevin Equation associated with the discrete biological phenomenon of the infection dynamics among "units" of susceptible individuals, subject to demographic noise. Immunity is assumed to be waning, meaning infection can recur after a recovery period. In other words, the ODE model is treated as the limit as $\Delta t \to 0$ of a jump Markov process $X(t) = (X_1(t),\ X_2(t))$, where $X_1(t) = S(t)$, $X_2(t) = I(t)$, describing the discrete stochastic process of SIS infection. For our simulation, the initial population size for each interacting species (susceptible and infected individuals) is set to 100 units. Following the formulation by Carletti and Banerjee [3], the system is governed by two underlying reaction channels, detailed below:

$$\begin{aligned} S + I &\to 2I \\ I &\to S \end{aligned} \tag{20}$$

The associated propensity functions $a_j(X)$, the stoichiometric vectors $\nu_j$, and reaction rates $c_j$ are defined as follows:

$$a_1(X) = c_1 X_1 X_2,\ a_2(X) = c_2 X_2;\ v_1 = [-1, 1]^T,\ v_2 = [1, -1]^T;\ c_1 = \beta/N,\ c_2 = \gamma. \tag{21}$$

Moreover, the Chemical Langevin Equation associated with the discrete system (20) and (21) takes the form of the following Itô SODE:

$$dX(t) = \sum_{j=1}^{2} v_j a_j(X(t))dt + B(X(t))dW(t), \quad X(0) = X_0 \tag{22}$$

where $W(t) = (W_1(t),\ W_2(t))^T$ is a 2-dimensional vector whose individual elements are independent Wiener processes, and $B(X(t))$ is a $2 \times 2$ matrix satisfying

$$B(X(t))B(X(t))^T = C(X(t)) = \nu Diag(a_1(X(t)), a_2(X(t)))v^T, \tag{23}$$

where $\nu = [\nu_1,\ \nu_2]$ is the $2 \times 2$ stoichiometric matrix. In the application of this approach to model (1), the terms $A = \sum v_j a_j$ and $B$ are associated with the drift and diffusion coefficients, respectively. In particular, computations show that the drift is the column vector

$$A = (-a_1(X) + a_2(X), a_1(X) - a_2(X))^T, \tag{24}$$

whereas the diffusion matrix $B$, such that $BB^T = C$, is obtained as the square root matrix of C, i.e.,

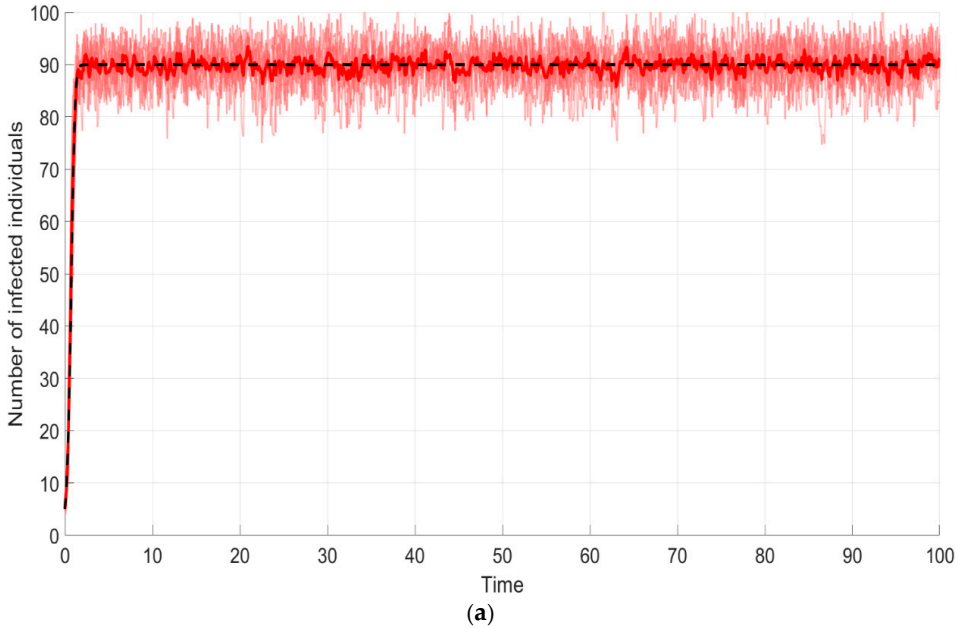
$$C = \begin{pmatrix} a_1 + a_2 & -a_1 - a_2 \\ -a_1 - a_2 & a_1 + a_2 \end{pmatrix} \tag{25}$$

Both paradigms (Allen's method and the backward technique) model demographic noise. Theoretically, the diffusion matrix (covariance structure) obtained through the backward approach should align with the one derived by Allen. In fact, the $C$ matrices (13) and (25), as well as the drift vectors in Equations (15) and (24), are identical. Analytically, both formulations describe the same Itô SODE system. Nevertheless, the algorithmic procedures differ fundamentally: while the forward method relies on SODE solvers (e.g., Euler's method), the backward framework evaluates the system trajectories by means of the SSA.

## 3. Numerical Results

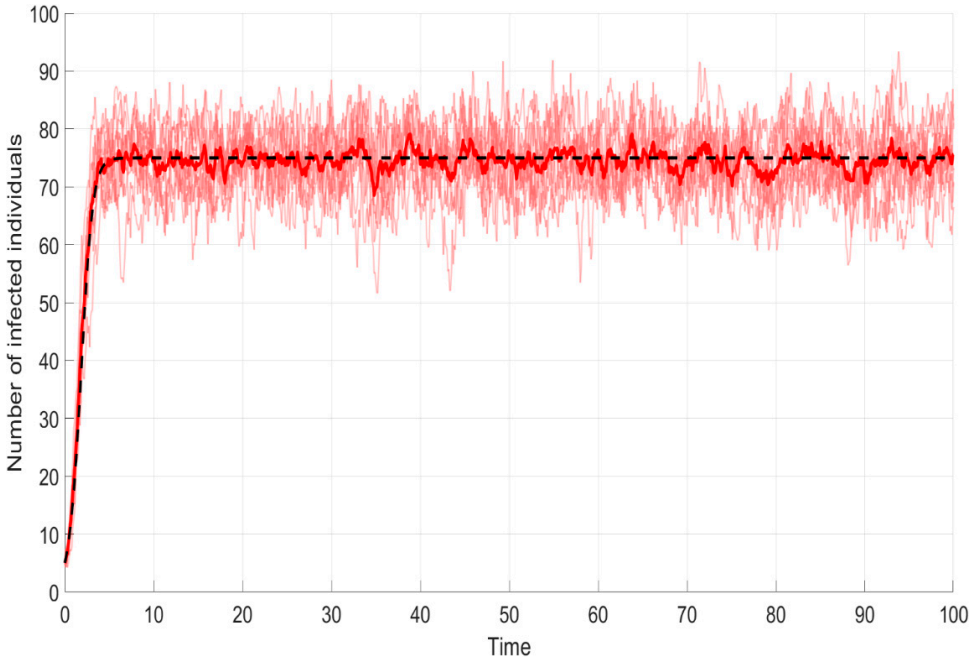
The numerical experiments presented in this paper were conducted on a latest-generation PC and implemented in the MATLAB R2026a environment running under Windows 11. For both Allen's method and the backward technique, the initial conditions were set to $S(0) = 95$ and $I(0) = 5$. These values represent population densities (units/volume) in the SODE resulting from Allen's method [2] and units in the SSA utilized for the backward technique. The compartmental volume $\Omega$ was assumed to be equal to 1.

The integration interval was set from 0 to 100 days, as the most significant dynamical transitions occur within this timeframe. For instance, when $\beta = 5, \gamma = 0.5$ (Figure 1a), the infected bacterial population rapidly reaches an endemic steady-state equilibrium of approximately 90 units/volume. As illustrated in Figure 1b–e, a decrease in the transmission parameter $\beta$ leads to a corresponding decline in the equilibrium values of the infected population. Notably, when $\beta < \gamma$, the infected population equilibrium vanishes in the long term.

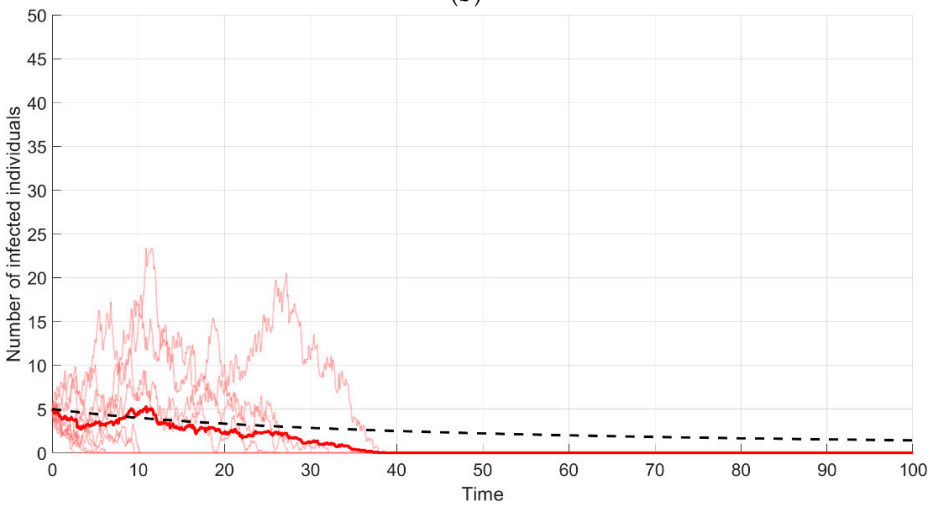



(**a**)

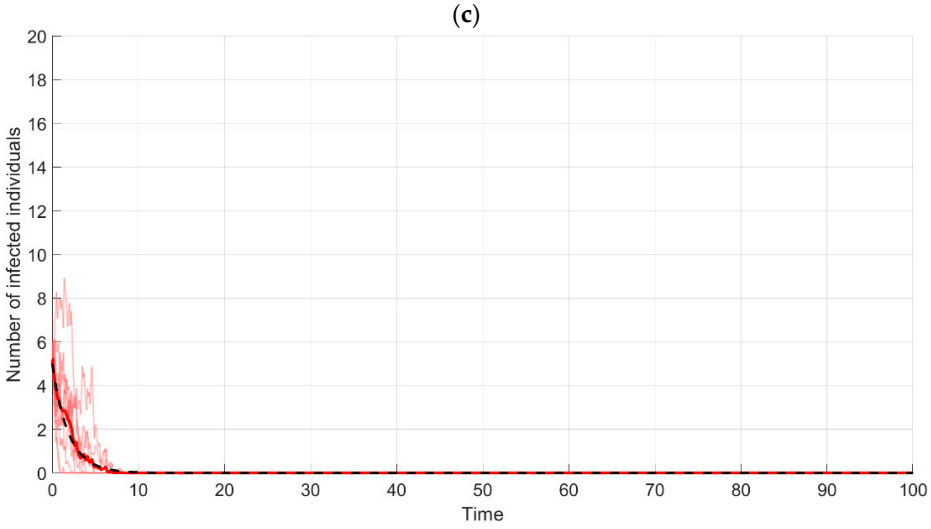
**Figure 1.** *Cont.*




(**b**)

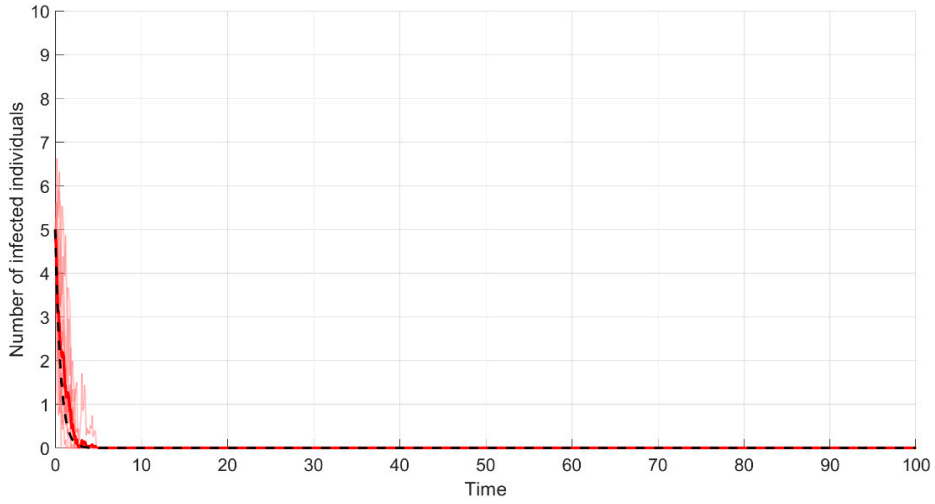



(**c**)

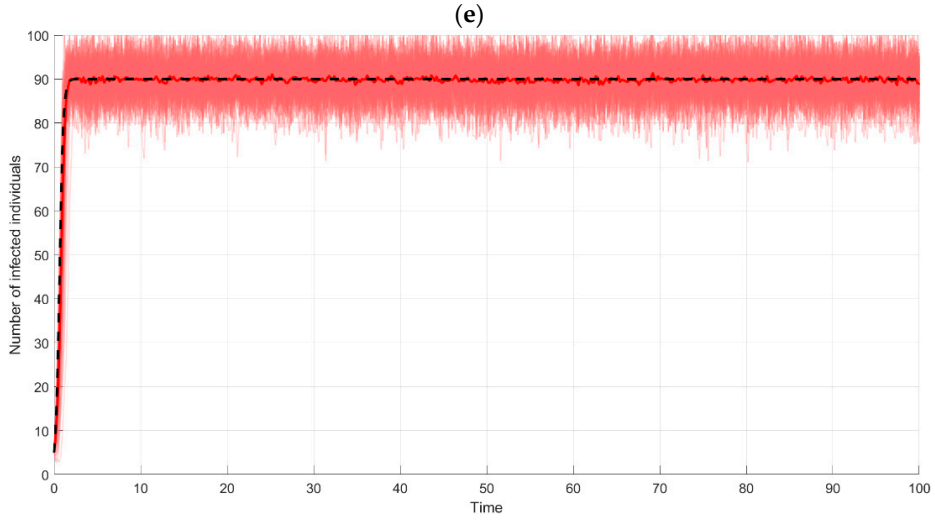



(**d**)

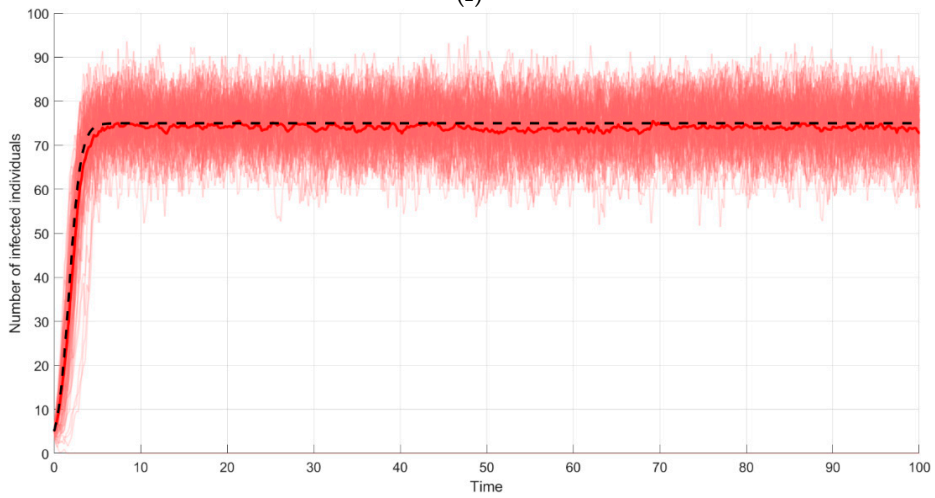
**Figure 1.** *Cont.*




(**e**)




(**f**)




(**g**)

**Figure 1.** *Cont*.

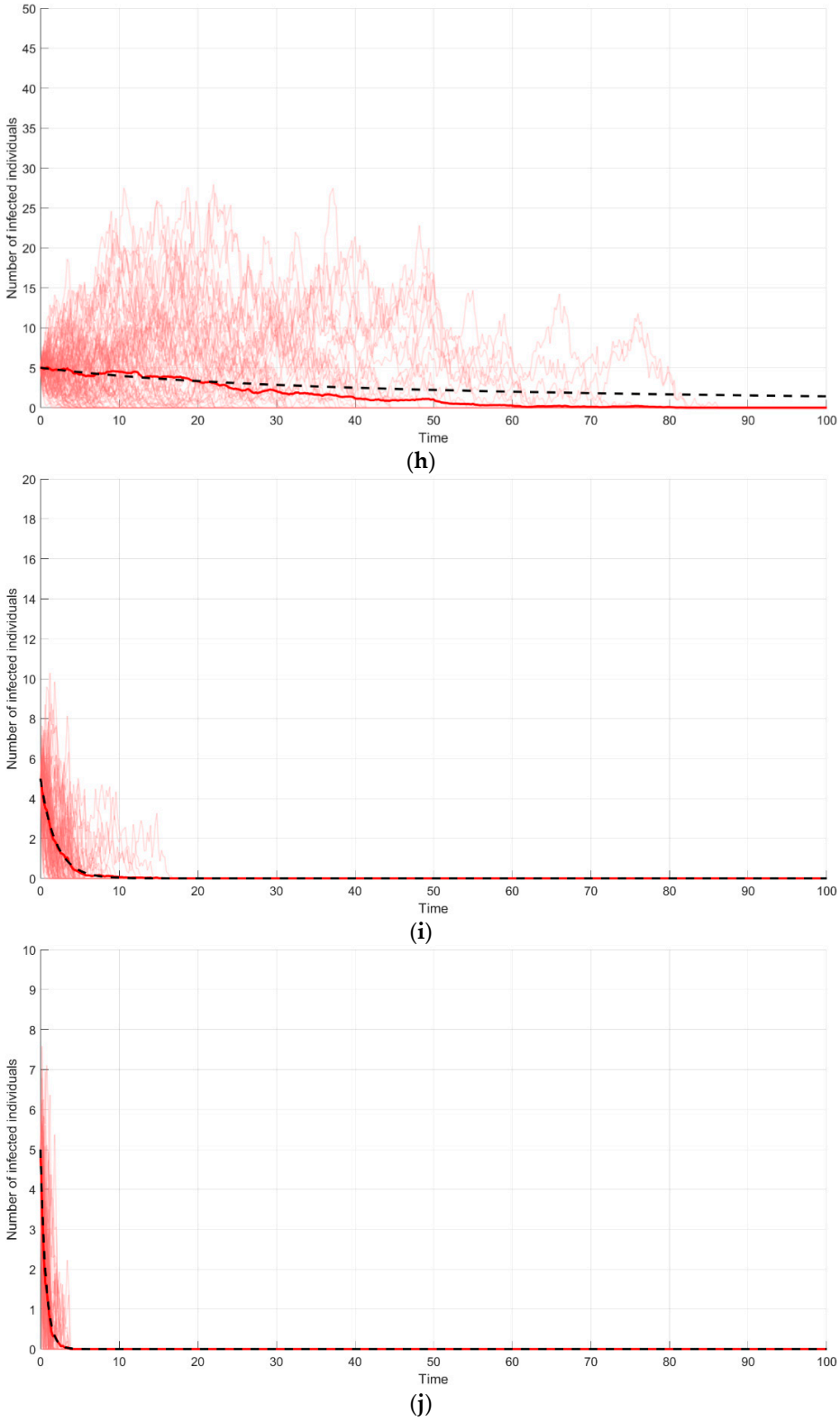



**Figure 1.** Time evolution of the infected population vector *I(t)* with time units in days on the horizontal axis and the number of individuals on the vertical axis. Initial conditions are set to *S(0)* = 95 and *I(0)* = *5* (units/volume for (**a**–**e**); units for (**f**–**j**)). (**a**–**e**) Simulations for model (15) using Allen's method, generated across M = 200 Brownian paths: (**a**) $\beta = 5$, $\gamma = 0.5$; (**b**) $\beta = 2$, $\gamma = 0.5$; (**c**) $\beta = 0.5$, $\gamma = 0.5$; (**d**) $\beta = 0.5$, $\gamma = 1$; (**e**) $\beta = 0.5$, $\gamma = 2$. (**f**–**j**) Simulations for models (20) and (21) using the backward technique: (**f**) $\beta = 5$, $\gamma = 0.5$; (**g**) $\beta = 2$, $\gamma = 0.5$; (**h**) $\beta = 0.5$, $\gamma = 0.5$; (**i**) $\beta = 0.5$, $\gamma = 1$; (**j**) $\beta = 0.5$, $\gamma = 2$.

Concerning Allen's method, we simulated the strong solutions of the Itô SODE (15) by means of the Euler–Maruyama method, computing the mean solution over $M = 200$ independent Brownian paths. For the backward technique, we simulated the stochastic discrete process [4,18] underlying the ODE (1) using the variant of Gillespie's SSA [5] developed by Burrage et al. [12] in the early 2000s.

In Figure 1a–e, we plot the mean solution of the SODE (15), while in Figure 1f–j, we display the discrete stochastic process (20) and (21) converging to the ODE (1) for different values of the parameters $\beta$ and $\gamma$. Although the parameter values for $\beta$ and $\gamma$ were chosen for illustrative purposes and do not refer to experimental data, their ranges were explicitly selected to encapsulate the full spectrum of epidemiological regimes defined in the literature on stochastic SIS models [19–21]. By scaling the basic reproduction number $R_0$ from subcritical conditions ($R_0 < 1$), through the critical threshold ($R_0 = 1$), up to highly supercritical regimes ($R_0 > 1$), this framework evaluates the numerical solvers across diverse physical behaviors.

Our analysis reveals that as the transmission parameter $\beta$ increases and $\beta > \gamma$, the two methods behave equivalently. However, Figure 1c–e,h–j show that this equivalence is slightly lost when $\beta \leq \gamma$. Taking into account that the SODEs (15) and (22) are analytically identical, it is crucial to distinguish between the theoretical equivalence of the continuous models and the numerical agreement of their implementations. Indeed, the observed discrepancies sample fundamentally different mathematical structures: an Euler–Maruyama continuous approximation of the SODE and an SSA simulation of the underlying discrete jump process.

For an SIS model without demographic renewal, $I = 0$ is an absorbing state; once $I = 0$, the propensities vanish ($a_1 = a_2 = 0$), making reinfection impossible [19]. When $\beta \leq \gamma$, the system frequently visits the neighborhood of this boundary. Under these regimes, standard Euler–Maruyama discretizations fail to preserve the positivity of the state space due to the non-globally Lipschitz nature of the diffusion coefficients, leading to negative values. The subsequent truncation (setting negative steps to zero) introduces a spurious numerical drift that artificially alters the extinction probability [22,23], compounding the structural mismatch between the continuous-state SDE and the underlying discrete Markov chain.

To mitigate these numerical artifacts and better capture the behavior near the boundary, several positivity-preserving numerical frameworks can be adopted. A prominent approach is the Lamperti-type transformation [24,25], which maps the state space to stabilize the square-root diffusion coefficient, preventing boundary violations without introducing spurious drift. Alternatively, Split-Step Backward Euler (SSBE) schemes [26] can handle the stiff absorbing boundary implicitly, while formulating a logarithmic transformation shifts the absorbing state to minus infinity, natively guaranteeing strict positivity. Lastly, truncated explicit variants of the Euler–Maruyama method [27,28] adjust the drift and diffusion operators near the boundary to preserve strong convergence.

To empirically validate these theoretical insights under the subcritical and critical regimes ($\beta \leq \gamma$), we systematically applied the Lamperti-type transformation to our continuous framework to investigate whether the observed discrepancies stem from algorithmic distortions or from fundamental modeling limits. Our computational experiments yield a critical insight: when comparing Allen's boundary-correction method in the original state space against its Lamperti-transformed counterpart, the resulting trajectories display remarkable quantitative and qualitative agreement. The fact that the Lamperti transformation does not significantly alter the profile of Allen's method proves that such explicit boundary corrections are already numerically robust and successfully free from spurious truncation artifacts.

Conversely, a stark and undeniable divergence emerges when comparing these stabilized, mathematically rigorous continuous profiles against the discrete backward framework (SSA). Because the Lamperti transformation guarantees that the continuous diffusion model is integrated without computational distortions, this remaining discrepancy cannot be dismissed as a numerical artifact. Therefore, we support the interpretation that the divergence between the continuous implementations (such as Allen's method) and the discrete backward technique (SSA) fundamentally reflects the intrinsic limitations of the diffusion approximation itself [22,29,30]. Under relatively small population sizes and in parameter regimes where stochastic fluctuations frequently drive the system toward the absorbing state, the continuous-state framework inherently fails to capture the discrete boundary dynamics of the underlying population process [29,30].

For parameter values where the two methods exhibit these slightly different behaviors, running multiple simulations of the SODEs (15) and (22) allows for a robust estimation of the ensemble statistics. To evaluate this numerical agreement rigorously, we introduced a Quasi-Stationary Analysis as a complementary quantitative framework, setting the number of sample paths to $M = 10,000$. Given this large ensemble size, the statistical uncertainty—measured via the Standard Error of the Mean (SEM) for the extinction times—is minimal, with all standard errors falling well below $O(10^{-2})$. This confirms that the observed quantitative differences between the two methods are statistically significant and cannot be attributed to stochastic sampling noise.

Our quantitative criterion for "agreement" relies on the qualitative and trend-wise consistency of the quasi-stationary state before the complete collapse of the system. As summarized in Table 2, when analyzing the time required for the active trajectories to drop to a fixed threshold (defined as 5% of the initial ensemble, i.e., 500 out of 10,000 active paths), both frameworks accurately track the same underlying physical behavior across the different parameter regimes.

**Table 2.** Average extinction times and quasi-stationary analysis for models (15) and (22) based on 10,000 Monte Carlo simulations, using a fixed Euler–Maruyama time step of $\Delta t = 10^{-3}$. The results compare Allen's forward method and the backward technique across different parameter combinations: $\beta = 0.5$ with $\gamma = 0.5$, 1, 2. Initial conditions are set to $S(0) = 95$, $I(0) = 5$, representing population densities (units/volume) in Allen's method and units in the backward technique. The standard error of the mean for the extinction time is $< 10^{-2}$. * Note: When the recovery rate $\gamma$ exceeds the contact rate $\beta$, all trajectories rapidly decay to zero. To capture the quasi-stationary distribution before the complete collapse of the system (i.e., before the histogram empties), the analysis is performed at the earliest time point where a sufficient threshold of active trajectories (at least 5%) remains available to ensure statistical validity.

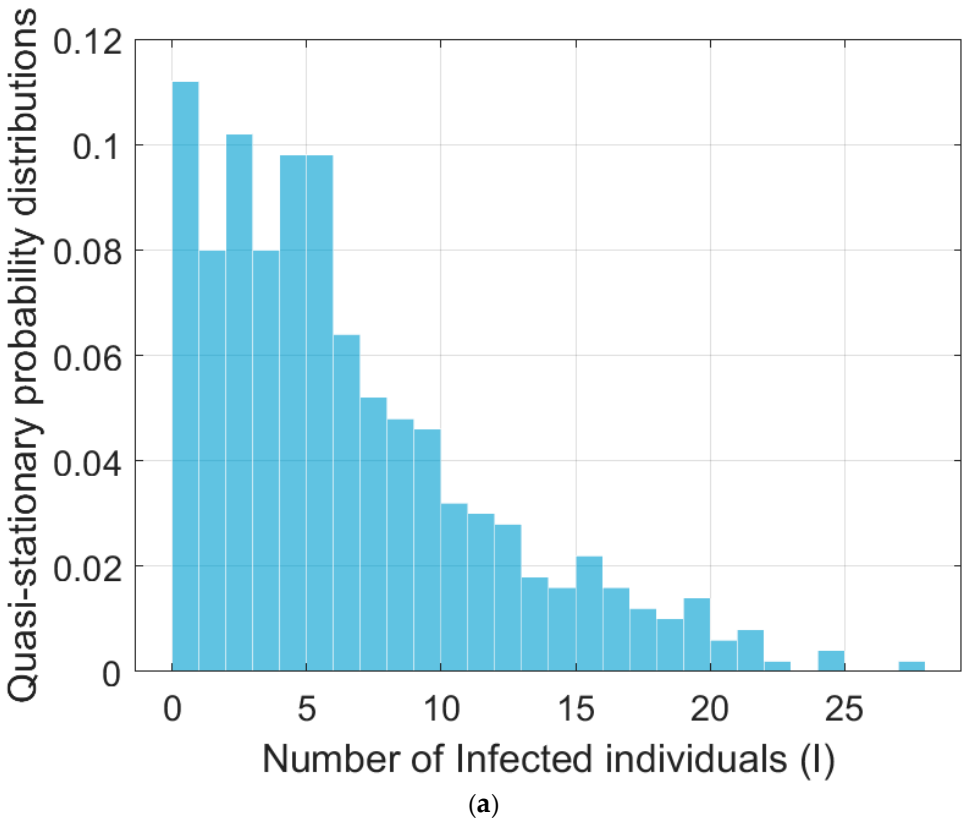
| | **Allen's Method** | | **Backward Technique** | |
|---|---|---|---|---|
| Parameters | The average extinction time | Quasi-Stationary Analysis * | The average extinction time | Quasi-Stationary Analysis * |
| $\beta = 0.5$, $\gamma = 0.5$ | 18.40 time units. Percentage of trajectories going extinct by T = 100: 99.71% | Trajectories still active at time t = 53.30: 500 out of 10,000 | 11.29 time units. Percentage of trajectories going extinct by T = 100: 100.00% | Trajectories still active at time t = 34.60: 504 out of 10,000 |
| $\beta = 0.5$, $\gamma = 1$ | 3.94 time units. Percentage of trajectories going extinct by T = 100: 100.00% | Trajectories still active at time t = 8.10: 515 out of 10,000 | 2.98 time units. Percentage of trajectories going extinct by T = 100: 100.00% | Trajectories still active at time t = 7.00: 502 out of 10,000 |

**Table 2.** *Cont.*

| | Allen's Method | | Backward Technique | |
|---|---|---|---|---|
| $\beta = 0.5$, $\gamma = 2$ | 1.59 time units. Percentage of trajectories going extinct by T = 100: 100.00% | Trajectories still active at time t = 3.20: 501 out of 10,000 | 1.24 time units. Percentage of trajectories going extinct by T = 100: 100.00% | Trajectories still active at time t = 2.80: 506 out of 10,000 |

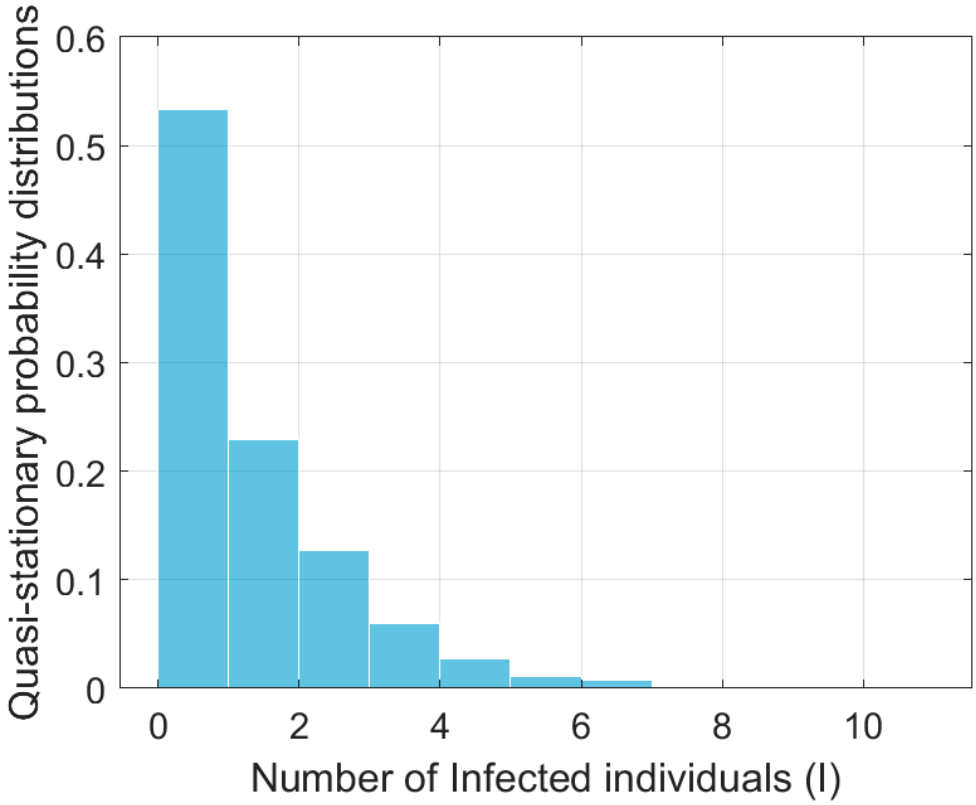
To ensure full transparency regarding the temporal discretization, the time step used for the Euler–Maruyama simulations ($\Delta t = 10^{-3}$) has been explicitly reported in the caption of Table 2. Furthermore, to verify that these findings are independent of the choice of discretization, we performed a comprehensive step-size convergence test by systematically reducing $\Delta t$ down to $10^{-5}$. The quantitative mismatch near the absorbing state persisted unaltered despite the finer temporal resolution. This confirms that the discrepancy is not a mere artifact of poor numerical discretization or time-step selection but is structurally rooted in the intrinsic limitations of the diffusion approximation itself near the absorbing boundary $I = 0$ when dealing with relatively small population sizes.

Crucially, it is worth noting that while increasing the number of simulated sample paths ($M$) reduces the statistical variance of the Monte Carlo estimators, the convergence of the stochastic system to the deterministic ODE (1) is instead theoretically driven by the large-population limit ($N \to \infty$) or the vanishing-noise limit, rather than the number of simulated paths (Table 2 and Figure 2a–f).

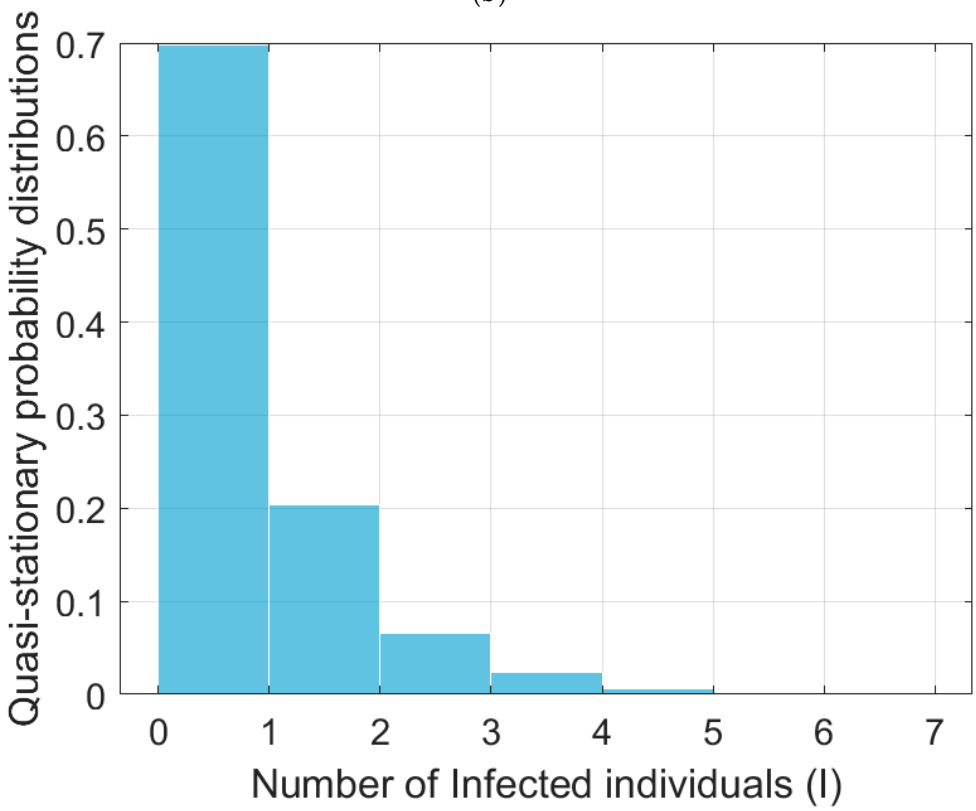



(**a**)

**Figure 2.** *Cont.*

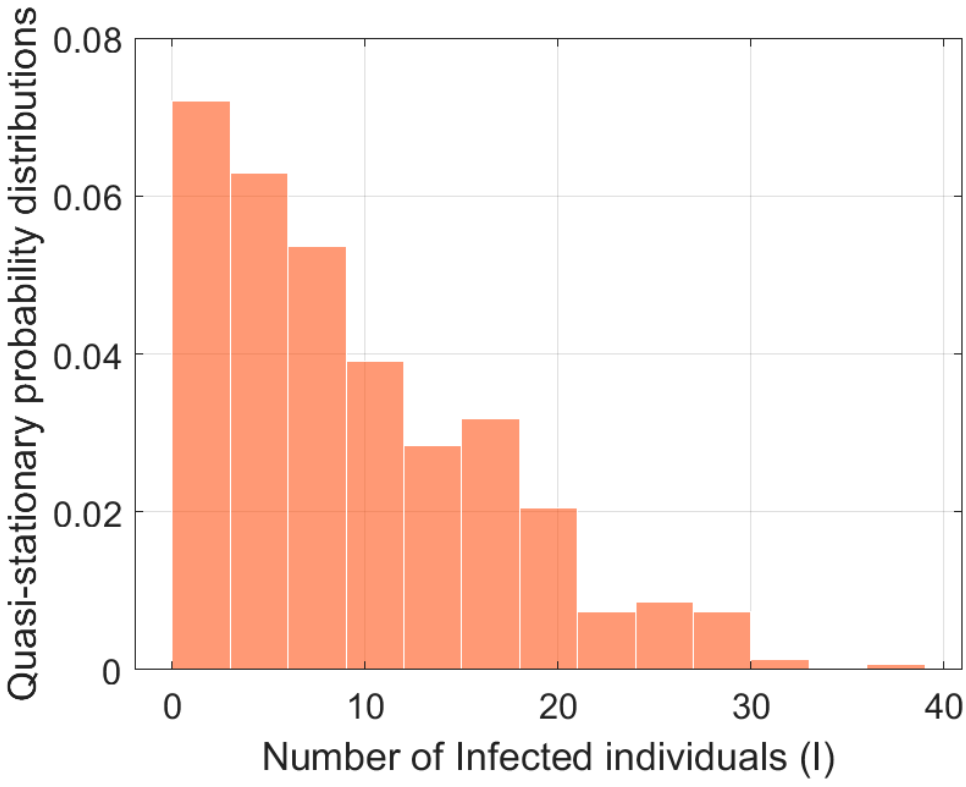



(**b**)

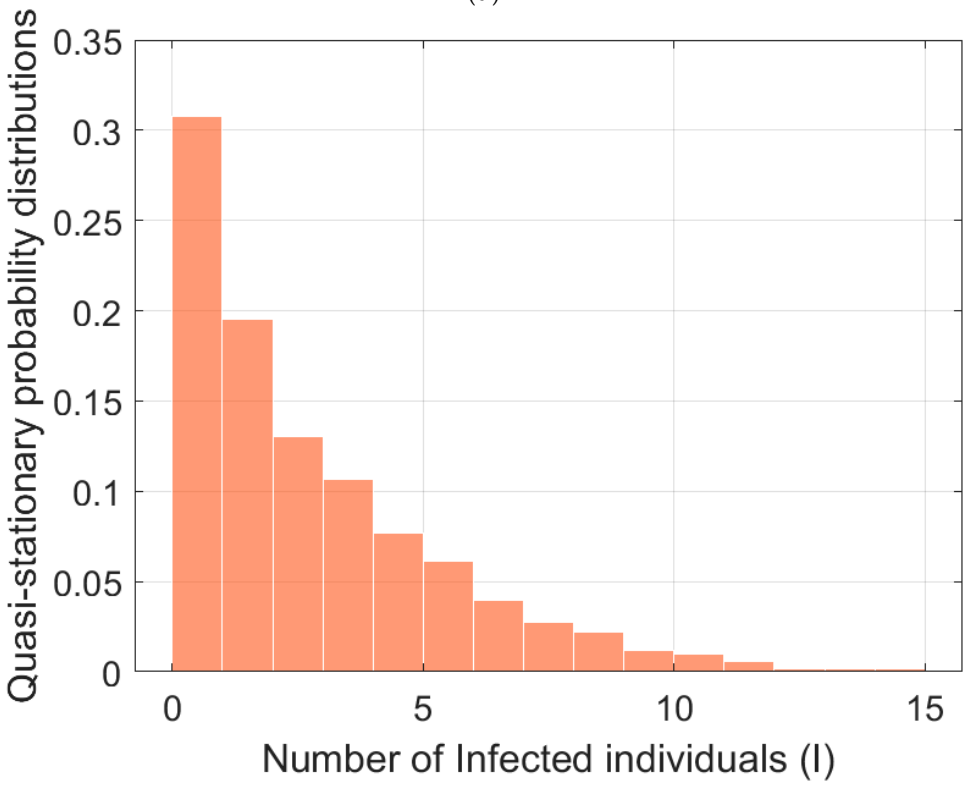



(**c**)

**Figure 2.** *Cont*.

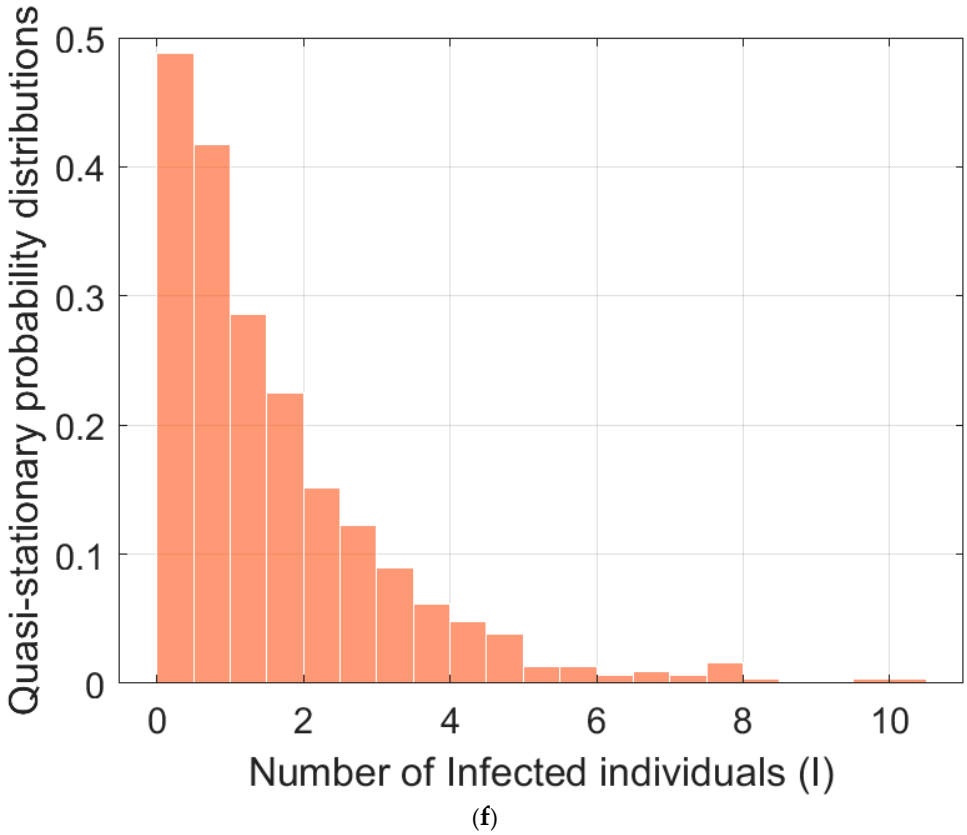



(**d**)




(**e**)

**Figure 2.** *Cont*.




(**f**)

**Figure 2.** Quasi-stationary probability distribution of the infected population vector *I(t)*. All distributions are generated from 10,000 Monte Carlo simulations using a fixed Euler–Maruyama time step of $\Delta t = 10^{-3}$ with $\beta = 0.5$. (**a**–**c**) Results for model (15) computed using Allen's method: (**a**) $\gamma = 0.5$; (**b**) $\gamma = 1$; (**c**) $\gamma = 2$. (**d**–**f**) Results for model (22) computed using the backward technique: (**d**) $\gamma = 0.5$; (**e**) $\gamma = 1$; (**f**) $\gamma = 2$.

## 4. Discussion

In this paper, we have presented a comparison between Allen's method [2] and the backward technique introduced by Carletti and Banerjee [3], both of which serve as powerful mathematical frameworks for modeling demographic noise in the life sciences. Allen's method begins with discrete stochastic processes, systematically deriving their continuous SODE counterparts embedded with intrinsic noise. Conversely, the backward technique infers and simulates the intrinsic noise of a biological phenomenon by mapping a continuous, deterministic differential system back to its underlying discrete stochastic process.

Our study indicates that while both methods capture qualitatively consistent dynamical trends—particularly within the supercritical regime—they exhibit noticeable quantitative discrepancies in their mean extinction times under critical and subcritical regimes $(\beta \leq \gamma)$, as summarized in Table 2. Given that SODEs (15) and (22) are analytically identical, it is crucial to distinguish between the theoretical equivalence of the continuous models and the numerical agreement of their implementations. Near the absorbing boundary $I = 0$, the combination of small population sizes and frequent boundary visitations exacerbates the structural differences between the continuous and discrete stochastic frameworks [22,23].

To rigorously investigate whether these discrepancies stem from numerical artifacts—such as positivity violations or the handling of the absorbing state—we systematically applied a Lamperti-type transformation to the continuous framework. This mathematical mapping transforms the multiplicative square-root noise into an additive

form, effectively stabilizing the integration near the boundary without altering the continuous nature of the SODE.

Crucially, our computational experiments revealed that the trajectories generated by Allen's method display remarkable qualitative and quantitative agreement with its Lamperti-transformed counterpart. This empirical finding provides strong numerical evidence that Allen's explicit boundary formulation is already numerically robust and successfully free from spurious truncation artifacts.

Conversely, a stark and undeniable divergence emerges when comparing these stabilized, mathematically rigorous continuous profiles against the discrete backward framework (SSA). Because the Lamperti transformation guarantees that the continuous diffusion model is integrated without computational distortions, this remaining discrepancy cannot be dismissed as a numerical artifact. Therefore, we support the interpretation that the divergence between the continuous Allen's method and the discrete backward technique (SSA) fundamentally reflects the intrinsic limitations of the diffusion approximation itself when driven frequently toward the absorbing state under relatively small population sizes.

Nevertheless, owing to its straightforward mathematical implementation compared to Allen's method, the backward technique remains a highly valuable tool. It enables the direct modeling of demographic noise by leveraging the extensive scientific literature and empirical data that are overwhelmingly dominated by continuous deterministic frameworks, such as systems of ODEs, expressed in terms of continuous densities rather than discrete counts. Consequently, this backward reconstruction technique proves to be highly versatile, offering a scalable methodology that can be readily extended to general ODE models across various scientific disciplines beyond the life sciences.

**Author Contributions:** Conceptualization, R.M. and M.C.; Methodology, R.M. and M.C.; Software, R.M. and M.C.; Validation, R.M. and M.C.; Formal analysis, R.M.; Investigation, R.M.; Resources, R.M.; Data curation, R.M.; Writing—original draft preparation, R.M.; Writing—review and editing, R.M. and M.C.; Visualization, R.M.; Supervision, R.M. and M.C.; Project administration, R.M. and M.C.; Funding acquisition, none. All authors have read and agreed to the published version of the manuscript.

**Funding:** This research received no external funding.

**Data Availability Statement:** The original contributions presented in this study are included in the article. Further inquiries can be directed to the corresponding author.

**Acknowledgments:** The authors would like to thank the anonymous referees for their valuable comments and suggestions, which greatly improved the quality of the manuscript.

**Conflicts of Interest:** The authors declare no conflict of interest.

## Appendix A

The deterministic SIS model equations are given by

$$\begin{cases} \frac{dS(t)}{dt} = -\frac{\beta}{N}S(t)I(t)+\gamma I(t) \\ \frac{dI(t)}{dt} = \frac{\beta}{N}S(t)I(t)-\gamma I(t) \end{cases}. \tag{A1}$$

To simplify the analysis, we introduce the dimensionless variables and parameters: $s = S/N, i = I/N, \tau = \beta t, k = \gamma/\beta = 1/R_0$. Subject to the conservation law $s(t) + i(t) = 1$, the system (A1) can be rewritten in the following consistent dimensionless form:

$$\begin{cases} \frac{ds(t)}{d\tau} = -s(\tau)i(\tau)+ki(\tau) \\ \frac{di(t)}{d\tau} = s(\tau)i(\tau)-ki(\tau) \end{cases}, \tag{A2}$$

where $s \geq 0, i \geq 0$, and the initial conditions are denoted as $(s(0), i(0)) = (s_0, i_0) \neq (0, 0)$. For $k \neq 1$, the explicit analytical solutions of the ODE system are as follows [31–36]:

$$s^*(\tau) = \frac{s_0 - k + k(1 - s_0)e^{(1-k)\tau}}{s_0 - k + (1 - s_0)e^{(1-k)\tau}}; i^*(\tau) = \frac{(1 - k)i_0 e^{(1-k)\tau}}{1 - k + i_0 e^{(1-k)\tau}} \tag{A3}$$

If $k = 1$ $(R_0 = 1)$, the solutions reduce to

$$s^*(\tau) = \frac{s_0 + (1 - s_0)\tau}{1 + (1 - s_0)\tau}; i^*(\tau) = \frac{i_0}{1 + i_0\tau} \tag{A4}$$

Consequently, if $k \geq 1$ $(R_0 \leq 1)$, we find that $\lim_{\tau\to\infty} s(\tau) = 1$, and $\lim_{\tau\to\infty} i(\tau) = 0$. Conversely, if $0 < k < 1$ $(R_0 > 1)$, the asymptotic limits are $\lim_{\tau\to\infty} s(\tau) = k$, $\lim_{\tau\to\infty} i(\tau) = 1 - k$.

Accordingly, the disease-free equilibrium (vanishing equilibrium) $E_0 = (1,\ 0)$ always exists. If $k \geq 1$, $E_0 = (1, 0)$ is globally asymptotically stable. If $0 < k < 1$, a unique positive endemic equilibrium $E_+ = (k, 1 - k)$ emerges and is globally asymptotically stable.

## References


1. Li, B.; Zhang, W.; Shi, M. A Distributionally Robust Optimization-Based Stochastic Self-Triggered Model Predictive Control. *IEEE Trans. Syst. Man Cybern. Syst.* **2026**, *56*, 2699–2707. [CrossRef]
2. Allen, L.J.S. *An Introduction to Stochastic Processes with Applications to Biology*, 2nd ed.; CRC Press: New York, NY, USA, 2010. [CrossRef]
3. Carletti, M.; Banerjee, M. A Backward Technique for Demographic Noise in Biological Ordinary Differential Equation Models. *Mathematics* **2019**, *7*, 1204. [CrossRef]
4. Burrage, K.; Tian, T. Effective simulation techniques for biological systems, in fluctuations and noise in biological, biophysical, and biomedical systems II. In *Proceedings of the SPIE—The International Society for Optical Engineering*; SPIE: Bellingham, WA, USA, 2004. [CrossRef]
5. Gillespie, D.T. A general method for numerically simulating the stochastic time evolution of coupled chemical reactions. *J. Comput. Phys.* **1976**, *22*, 403–434. [CrossRef]
6. Bailey, N.T.J. *The Elements of Stochastic Processes with Applications to the Natural Sciences*; John Wiley & Sons: New York, NY, USA, 1990.
7. Mandal, P.S.; Allen, L.J.S.; Banerjee, M. Stochastic Modeling of Phytoplankton Allelopathy. *Appl. Math. Model.* **2014**, *38*, 1583–1596. [CrossRef]
8. Allen, E. *Modeling with Itô Stochastic Differential Equations*; Springer: Dordrecht, The Netherlands, 2007. [CrossRef]
9. Allen, E.J.; Allen, L.J.S.; Arciniega, A.; Greenwood, P. Construction of equivalent stochastic differential equation models. *Stoch. Anal. Appl.* **2008**, *26*, 274–297. [CrossRef]
10. Kurtz, T.G. Limit theorems for sequences of jump Markov processes approximating ordinary differential processes. *J. Appl. Probab.* **1971**, *8*, 344–356. [CrossRef]
11. Cao, Y.; Li, H.; Petzold, L. Efficient formulation of the stochastic simulation algorithm for chemically reacting systems. *J. Chem. Phys.* **2004**, *121*, 4059–4067. [CrossRef] [PubMed]
12. Burrage, K.; Tian, T.; Burrage, P. A multi-scaled approach for simulating chemical reaction systems. *Prog. Biophys. Mol. Biol.* **2004**, *85*, 217–234. [CrossRef] [PubMed]
13. Arkin, A.; Ross, J.; McAdams, H.H. Stochastic kinetic analysis of developmental pathway bifurcation in phage lambda-infected Escherichia coli cells. *Genetics* **1998**, *149*, 1633–1648. [CrossRef] [PubMed]
14. Elowitz, M.B.; Leibler, S. A synthetic oscillatory network of transcriptional regulators. *Nature* **2000**, *403*, 335–338. [CrossRef] [PubMed]
15. Gonze, D.; Halloy, J.; Goldbeter, A. Robustness of circadian rythms with respect to molecular noise. *Proc. Natl. Acad. Sci. USA* **2002**, *99*, 673–678. [CrossRef] [PubMed]
16. Gillespie, D.T. A rigorous derivation of the chemical master equation. *Physica A* **1992**, *188*, 404–425. [CrossRef]
17. Allen, L.J.S. Some discrete-time SI, SIR, and SIS epidemic models. *Math. Biosci.* **1994**, *124*, 83–105. [CrossRef] [PubMed]
18. Burrage, K.; Burrage, P.; Leier, A.; Marquez-Lago, T.A.; Marquez-Lago, T. A review of stochastic and delay simulation approaches in both time and space in computational cell biology. In *Stochastic Processes, Multiscale Modeling, and Numerical Methods for Computational Cellular Biology*; Holcman, D., Ed.; Springer: New York, NY, USA, 2017. [CrossRef] [PubMed]

19. Allen, L.J. An Introduction to Stochastic Epidemic Models. In *Mathematical Epidemiology*; Brauer, F., van den Driessche, P., Wu, J., Eds.; Springer: Berlin/Heidelberg, Germany, 2008; pp. 81–130. [CrossRef]
20. Gray, A.; Greenhalgh, D.; Hu, L.; Mao, X.; Pan, J. A stochastic differential equation SIS epidemic model. *SIAM J. Appl. Math.* **2011**, *71*, 876–902. [CrossRef]
21. Pan, J.; Gray, A.; Greenhalgh, D.; Mao, X. Parameter estimation for the stochastic SIS epidemic model. *Stat. Inference Stoch. Processes* **2014**, *17*, 75–98. [CrossRef]
22. Higham, D.J.; Mao, X.; Stuart, A.M. Strong convergence of Euler–like methods for nonlinear stochastic differential equations. *SIAM J. Numer. Anal.* **2002**, *40*, 1041–1063. [CrossRef]
23. Lord, G.J.; Powell, C.E.; Shardlow, T. *An Introduction to Computational Stochastic PDEs*; Cambridge University Press: Cambridge, UK, 2014. [CrossRef]
24. Mao, X.; Szpruch, L. Strong convergence and stability of implicit numerical methods for stochastic differential equations with non-globally Lipschitz continuous coefficients. *J. Comput. Appl. Math.* **2013**, *238*, 14–28. [CrossRef]
25. Liu, R.; Wang, X. A higher order positivity preserving scheme for the strong approximations of a stochastic epidemic model. *Commun. Nonlinear Sci. Numer. Simul.* **2023**, *124*, 107258. [CrossRef]
26. Higham, D.J.; Mao, X.; Stuart, A.M. Exponential mean-square stability of numerical solutions to stochastic differential equations. *LMS J. Comput. Math.* **2003**, *6*, 297–313. [CrossRef]
27. Mao, X. The truncated Euler–Maruyama method for stochastic differential equations. *J. Comput. Appl. Math.* **2015**, *290*, 370–384. [CrossRef]
28. Hutzenthaler, M.; Jentzen, A.; Kloeden, P.E. Strong convergence of an explicit numerical method for SDEs with nonglobally Lipschitz continuous coefficients. *Ann. Appl. Probab.* **2012**, *22*, 1611–1641. [CrossRef]
29. Nasell, I. Stochastic Models of Some Endemic Infections. *Math. Biosci.* **2002**, *179*, 1–19. [CrossRef] [PubMed]
30. Fuchs, C. *Inference for Diffusion Processes: With Applications in Life Sciences*; Springer Science & Business Media: Berlin/Heidelberg, Germany, 2013. [CrossRef]
31. Mascia, C.; Montefusco, E. Modelli Deterministici in Epidemiologia, Corso di Modelli Analitici per Applicazioni. Available online: https://web.unica.it/static/resources/cms/documents/modan2_2.pdf (accessed on 1 August 2026).
32. Bailey, N.T.J. *The Mathematical Theory of Infectious Diseases and Its Applications*, 2nd ed.; Hafner Press [Macmillan Publishing Co., Inc.]: New York, NY, USA, 1975.
33. Capasso, V. *Mathematical Structures of Epidemic Systems*; Lecture Notes in Biomathematics; Springer: Berlin/Heidelberg, Germany, 1993; Volume 97. [CrossRef]
34. Cesari, L. *Asymptotic Behavior and Stability Problems in Ordinary Differential Equations*, 3rd ed.; Ergebnisse der Mathematik und ihrer Grenzgebiete, Band 16; Springer: New York, NY, USA; Berlin/Heidelberg, Germany, 1971. [CrossRef]
35. Hethcote, H.W. The mathematics of infectious diseases. *SIAM Rev.* **2000**, *42*, 599–653. [CrossRef]
36. Korobeinikov, A.; Wake, G.C. Lyapunov functions and global stability for SIR, SIRS, and SIS epidemiological models. *Appl. Math. Lett.* **2002**, *15*, 955–960. [CrossRef]


**Disclaimer/Publisher's Note:** The statements, opinions and data contained in all publications are solely those of the individual author(s) and contributor(s) and not of MDPI and/or the editor(s). MDPI and/or the editor(s) disclaim responsibility for any injury to people or property resulting from any ideas, methods, instructions or products referred to in the content.